

1 **Reactivity of homoleptic and heteroleptic core paddle wheel Cu(II) compounds**

2
3
4
5
6
7
8
9
10
11
12
13
14
15
16
17
18
19
20
21
22
23
24
25
26
27
28
29
30
31
32
33
34
35
36
37
38
39
40
41
42
43
44

Francisco Sánchez-Férez^a, Miguel Guerrero^a, José A. Ayllón^a, Teresa Calvet^b, Mercè Font-Bardia^c,
José Giner Planas^d, Josefina Pons^{a,*}

- a Departament de Química, Universitat Autònoma de Barcelona, 08193-Bellaterra, Barcelona, Spain
b Mineralogia, Petrologia I Geologia Aplicada, Universitat de Barcelona, Martí I Franquès s/n, 08028-
Barcelona, Spain
c Unitat de Difracció de Raig-X, Centres Científics I Tecnològics de la Universitat de Barcelona
(CCiTUB), Universitat de Barcelona, Solé i Sabarís, 1-3, 08028-Barcelona, Spain
d Instituto de Ciencia de los Materiales de Barcelona (CSIC), Campus UAB, 08193 Bellaterra, Spain

josefina.pons@uab.cat (J. Pons).

45 **ABSTRACT:**

46

47 The compound $[\text{Cu}(\mu\text{-Pip})(\mu\text{-OAc})(\text{MeOH})_2]$ (1) (Pip=Piperonylate, OAc=acetate, MeOH=methanol)
48 has been obtained in high percentage yield. Its reactivity with pyridine/pyrazole derivative ligands
49 (pyridine (py), 3-phenylpyridine (3-Phpy) and 4-acetylpyridine (4-Acpy)) and 3,5-dimethylpyrazole
50 (3,5-dmpz) leads to four monomeric compounds: $[\text{Cu}(\text{Pip})_2(\text{dPy})_2(\text{H}_2\text{O})]$ (dPy=py (2), 3-Phpy (3) and
51 4-Acpy (4a)) and $[\text{Cu}(\text{Pip})_2(3,5\text{-dmpz})_2]$ (5). Furthermore, the reaction of 1 with HPip in MeOH:DMF
52 solvent under reflux conditions yields the homoleptic core paddle-wheel compound $[\text{Cu}(\mu\text{-}$
53 $\text{Pip})_2(\text{DMF})_2] \cdot 2\text{DMF}$ (6). The reaction between 6 and 2-benzylpyridine (2-Bzpy) yields the paddle-
54 wheel core compound $[\text{Cu}(\text{Pip})_2(2\text{-Bzpy})_2]$ (7). All compounds have been fully characterized by
55 analytical and spectroscopic techniques and their X-ray crystal structures have been determined. In this
56 set of compounds, the carboxylate ligand (Pip) displays different coordination modes (monodentate (2–
57 4), bidentate chelate (5) and bridged (1, 6 and 7)). Moreover, their extended structures are discussed: the
58 crystal packing indicates hydrogen bond propagation, which defines 1D (2–5) or 2D (6 and 7)
59 supramolecular networks.

60 ..

61 1. INTRODUCTION

62

63 The synthesis and characterization of crystalline materials buildup by covalent bonds has gained an
64 important interest, especially, the association of molecular compounds to form extended solids starting
65 from secondary building units (SBUs) [1,2]. The assembly of metalcarboxylates for constructing new
66 SBUs is an extensively exploited research field. These kind of compounds play an important role in
67 synthetic chemistry, thanks to their labile coordination mode and even more important, in the design of
68 porous frameworks [3].

69 Supramolecular chemistry is also an emergent research area, providing new complexes, which form
70 chemical systems different from those linked with covalent bonds. These systems are composed of two
71 or more assembled molecular subunits joined by relatively weak intermolecular forces (hydrogen bond,
72 hydrophobic and π -interactions, van der Waals forces, and electrostatic effects) [1,4].

73 An important family of SBUs are Cu(II) and Zn (II) paddle-wheel complexes. There are >1400 crystal
74 structures containing Cu(II) with a $[\text{Cu}_2\text{L}_4]$ (L=R-COO) homoleptic core [5]. From those, only twelve
75 present mixed bridged carboxylates $[\text{Cu}(\text{L})(\text{L}')(\text{X})_2]$ [6–16] in which six structures are accomplished via
76 acetate bridging units [8–11,13,14]. There is not a rigorous explanation for its formation; steric hindrance
77 could only play a significant role in three of them [11,13]. Recently, we have been studying the role of
78 carboxylic acids in the structural arrangement. In this sense, reactions with 4-hydroxybenzoic acid
79 (HpOHBz), (E)-3-(4-hydroxyphenyl)-2-propenoic acid (para-hydroxycinnamic acid, HpOHcinn) and
80 1,3-benzodioxole-5-carboxylic acid (Piperonylic acid, HPip) with Cu(II) [17–20], Zn(II) [21] and Cd(II)
81 [21] have already been studied.

82 Herein, we focus on this novel compound with an heteroleptic paddle-wheel core $[\text{Cu}(\mu\text{-Pip})(\mu\text{-}$
83 $\text{OAc})(\text{MeOH})_2]$ (1) (OAc=acetate), recently obtained in our research group [18]. Homoleptic core
84 paddlewheel have been vastly used as starting building units for the design of supramolecular [6] or
85 polymeric [22] architectures while there is not any research with those containing a heteroleptic paddle-
86 wheel core. Herewith, the reactivity of 1 with pyridine/pyrazole derivative ligands (pyridine (py, 2); 3-
87 phenylpyridine (3-Phpy, 3); 4-acetylpyridine (4-Acpy, 4) and 3,5-dimethylpyrazole (3,5-dmpz, 5)) have
88 been studied, resulting in monomeric compounds $[\text{Cu}(\text{Pip})_2(\text{dPy})_2(\text{H}_2\text{O})]$ (2–5). The displacement of
89 the two remaining acetate units of 1 allow us to reach the homoleptic paddle-wheel
90 $[\text{Cu}(\text{Pip})_2(\text{DMF})_2 \cdot 2\text{DMF}]$ (6) and gives us the possibility to perform further reactivity with 2-
91 benzylpyridine ligand (2-Bzpy), which yields $[\text{Cu}(\text{Pip})_2(2\text{-Bzpy})_2]$ (7) (Scheme 1).

92

93 2. EXPERIMENTAL SECTION

94

95 2.1. Materials and methods

96

97 Cu(II) acetate monohydrate (Cu(OAc)₂·H₂O), 1,3-benzodioxole-5-carboxylic acid (piperonylic acid,
98 HPip), pyridine (py), 3-phenylpyridine (3-Phpy), 4-acetylpyridine (4-Acpy), 2-benzylpyridine (2-Bzpy)
99 and 3,5-dimethylpyrazole (3,5-dmpz) ligands; methanol (MeOH), N,N-dimethylformamide (DMF) and
100 hexane were used as solvents. All of them were purchased from Sigma-Aldrich and used without further
101 purification. Reactions and manipulation were carried out in air at room temperature (r.t.) for
102 compounds 1–3 and under reflux conditions for 4–7. Elemental analysis (C, H, N) were carried out on a
103 Thermo Scientific Flash 2000 CHNS Analyser. The ATR-FTIR spectra were recorded on a Perkin
104 Elmer spectrometer, equipped with a universal attenuated total reflectance (ATR) accessory with
105 diamond window in the range 4000–550 cm⁻¹. The electronic spectra in solution of MeOH (≈ 1·10⁻³
106 M) were run on a spectrophotometer Cary 500 Varian, equipped with a quartz cell having a path length
107 of 1 cm in the range of 500–800 nm. Powder X-ray diffraction (PXR) patterns were measured with a
108 Siemens D5000 apparatus (with 40 kW and 45 mA using CuK α radiation with λ =1.5406 Å). All of them
109 were recorded from 2 θ =5° to 30° with a step scan of 0.02° counting 1s at each step.

110

111 2.2. Synthetic procedures

112

113 2.2.1. [Cu(μ -Pip)(μ -OAc)(MeOH)]₂ (1)

114 To a solution containing HPip (503 mg, 3.03 mmol) in MeOH (120 mL), the green powder
115 Cu(OAc)₂·H₂O (550 mg, 3.03 mmol) was added portion wise and stirred for 5 h at r.t, a green
116 precipitate appeared immediately. The product was filtered off, washed with 10 mL of cold methanol
117 and dried on air. Yield: 865 mg (89%). The same reaction was also performed in presence of AcOH acid
118 (3.0 mL) with similar yield (845 mg, 87%) (S.I.: Fig. S1). Elem. Anal. Calc. for C₂₂H₂₄O₁₄Cu₂
119 (639.52 g/mol): C 41.32; H 3.78. Found: C 41.05; H 3.54%. ATR-FTIR (wavenumber, cm⁻¹): 3301(m)
120 [ν (OeH)]MeOH, 3060(w) [ν (C-H)], 2955(w) [ν (C-H)], 1628(m), 1593(s) [ν (C=O)], 1508(w)
121 [ν (C-C)], 1493(m), 1442(s) [ν (C=O)], 1390(s), 1356(m), 1265(s) [δ (OH)], 1244(m), 1174(w),
122 1117(m) [ν (C-O-C)], 1079(w), 1036(m), 1022(s) [δ (C-H)], 935(w), 922(m), 884(w), 804(m), 775(s)
123 [δ (oop)(C-H)], 684(s) [δ (oop)(C-H)], 628(m). UV-Vis (Methanol, 1.1·10⁻³M) λ _{max} (ϵ)=716 (1 2 4) nm.

124

125 2.2.2. [Cu(Pip)₂(py)₂(H₂O)] (2)

126 To a solution containing 1 (100 mg, 0.156 mmol) in MeOH (40 mL), a solution of py (0.25 mL, 3.13
127 mmol) in MeOH (10 mL) was added dropwise and stirred for 1 h. The solution turned dark blue and was
128 subjected to several cooling-evaporation cycles. The resulting blue powder was filtered off, washed with
129 10 mL of cold methanol and dried on air. Suitable blue crystals were obtained after evaporation of

130 mother liquors on air for 10 days. Yield: 55.2 mg (62%). Elem. Anal. Calc. for C₂₆H₂₂N₂O₉Cu
131 (569.99 g/mol): C 54.78; H 3.89; N 4.91. Found: C 54.92; H 3.75; N 4.84%. ATR-FTIR (wavenumber,
132 cm⁻¹): 3291(w) [v(OeH)]water, 3071(w) [var(CeH)], 2909(w) [val(CeH)], 1607(m), 1579(s)
133 [vas(COO)], 1566(s), 1501(m), 1487(m), 1448(m), 1434(s) [vs(COO)], 1379(s), 1346(s), 1255(s),
134 1239(s), 1220(m) [δ(OH)], 1166(m), 1109(m) [v(CeOeC)], 1073(m), 1035(s) [δip(CeH)], 934(m),
135 918(m), 802(m), 770(s) [δoop(CeH)], 722(m), 705(s), 696(s), 678(s), 635(s), 607(s), 583(s). UV-Vis
136 (Methanol, 9.7·10⁻⁴ M) λ_{max} (ε)=710 (33) nm.

137

138 2.2.3. [Cu(Pip)₂(3-Phpy)₂(H₂O)] (3)

139 To a solution containing 3-Phpy (226 mg, 0.313 mmol) in MeOH (10 mL), a green solution of 1 (100
140 mg, 0.156 mmol) in MeOH (30 mL) was added dropwise and stirred for 1 h. The solution turned dark
141 blue and was treated as 2. Suitable blue crystals were obtained after evaporation of the mother liquors on
142 air for 20 days. Yield: 63.3 mg (56%). Elem. Anal. Calc. for C₃₈H₃₀N₂O₉Cu (722.18 g/mol): C 63.20;
143 H 3.19; N 3.88. Found: C 63.05; H 3.25; N 3.72%. ATR-FTIR (wavenumber, cm⁻¹): 3241(br)
144 [v(OeH)]water, 3085(w) [var(CeH)], 2919(w) [val(CeH)], 1569(s) [vas(COO)], 1500(w), 1476(w),
145 1439(s), 1362(s) [vs(COO)], 1257(m), 1236(s), 1210(m) [δ(OH)], 1111(m) [v(CeOeC)], 1034(s)
146 [δip(CeH)], 919(s), 801(m), 777(s) [δoop(CeH)], 752(s) [δoop(CeH)], 702(s), 686(m), 682(m), 583(m).
147 UV-Vis (Methanol, 1.3·10⁻³ M) λ_{max} (ε)=727 (78) nm.

148

149 2.2.4. [Cu(Pip)₂(4-Acpy)₂(H₂O)]·3MeOH·H₂O (4a)

150 To a solution containing 4-Acpy (37.9 mg, 0.313 mmol) in MeOH (10 mL), a green solution of 1 (100
151 mg, 0.156 mmol) in MeOH (30 mL) was added dropwise and stirred under reflux conditions for a day.
152 The resulting dark green powder was filtered off, washed with 10 mL of cold methanol and dried under
153 vacuum. Suitable blue crystals were obtained by slow evaporation of mother liquors on air for 14 days.
154 The stoichiometry of this compound was definitely established after resolution of their X-ray crystal
155 structure. However, the occluded solvent molecules are withdrawn from the structure after manipulation
156 required for preparing the sample for EA yielding [Cu(Pip)₂(4-Acpy)₂(H₂O)] (4b).

157 4a. Yield: 98.2 mg (82%). C₃₃H₄₀N₂O₁₅Cu (768.25 g/mol). ATRFTIR (wavenumber, cm⁻¹): 3350(m)
158 and 3265(m) ([v(OeH)]MeOH+[v(OeH)]water), 3055(w) [var(CeH)], 2917(m) [val(CeH)], 1696(s)
159 [v(C)O]4-Acpy, 1660(w), 1568(s) [vas(COO)], 1506(m), 1492(w), 1440(s), 1419(s) [vs(COO)],
160 1357(s), 1258(s), 1242(s), 1227(s) [δ(OH)], 1205(m), 1168(m), 1132(w), 1115(m) [v(CeOeC)], 1076(w),
161 1062(m), 1031(s) [δip(CeH)], 993(w), 962(w), 919(s), 891(m), 830(m), 819(s), 802(m), 777(s)
162 [δoop(CeH)], 721(m), 676(m), 592(s), 585(s). 4b. Yield: 83.1 mg (82%). Elem. Anal. Calc. for
163 C₃₀H₂₆N₂O₁₁Cu (636.09 g/mol): C 55.09; H 4.01; N 4.28. Found: C 55.23; H 4.30; N 4.40%. ATR-
164 FTIR (wavenumber, cm⁻¹): 3049(m) [var(CeH)], 2919(w) [val(CeH)], 1699(s) [v(C)O]4-Acpy,
165 1622(s), 1558(s) [vas(COO)], 1506(m), 1492(m), 1445(s), 1413(s), 1355(s), 1260(s), 1230(m), 1145(m),
166 1120(m) [v(CeOeC)], 1082(w), 1062(w), 1029(m) [δip(CeH)], 993(w), 961(w), 920(m), 870(m),

167 844(m), 821(m), 777(s) [δ oop(CeH)], 742(w), 696(m), 669(m). UV-Vis (Methanol, $9.9 \cdot 10^{-4}$ M) λ_{\max}
168 (ϵ)=677 (68) nm.

169

170 2.2.5. [Cu(Pip)₂(3,5-dmpz)₂] (5)

171 To a solution containing 3,5-dmpz (30.1 mg, 0.313 mmol) in MeOH (15 mL), a green solution of 1 (100
172 mg, 0.156 mmol) in MeOH (25 mL) was added dropwise and stirred under reflux conditions for 1 h. The
173 solution was evaporated almost half of the volume and a violet powder was formed. The powder was
174 filtered and washed with 10 mL of cold MeOH. Suitable violet crystals were obtained by slow
175 evaporation of mother liquors on air for 5 days. Yield: 48.6 mg (53%). Elem. Anal. Calc. for
176 C₃₈H₃₀CuN₂O₉ (586.05 g/mol): C 53.29; H 4.47; N 9.56. Found: C 53.17; H 4.35; N 9.45%. ATR-
177 FTIR (wavenumber, cm⁻¹): 3186-3105(br) [ν (NeH)], 3036(w) [ν ar(CeH)], 2929(w)-2879(br)
178 [ν al(CeH)], 2783(w), 1631(w), 1604(w), 1557(s) [ν as(COO)], 1501(s), 1486(m), 1435(m) [ν s(COO)],
179 1381(s), 1341(s), 1300(m), 1257(m), 1240(s), 1189(m), 1166(w), 1143(w), 1113(m) [ν (CeOeC)],
180 1075(w), 1059(m), 1034(s) [δ ip(CeH)], 989(w), 935(m), 921(s), 887(m), 825(m), 805(s), 775(s)
181 [δ oop(CeH)], 740(m), 721(m), 685(m), 665(w), 640(w), 593(m/s), 560(m). UV-Vis: (Methanol,
182 $9.5 \cdot 10^{-4}$ M) λ_{\max} (ϵ)=714 (13) nm.

183

184 2.2.6. [Cu(Pip)₂(DMF)₂·2DMF] (6)

185 Method A. To a colourless solution of HPip (51.9 mg, 0.313 mmol) in MeOH:DMF (2.5:1; 35 mL), the
186 green powder of 1 (100 mg, 0.157 mmol) was added and stirred under reflux conditions at 120 °C for 48
187 h. The colour of the solution changed from green to dark blue. The resultant solution was treated with
188 the sequential cooling-evaporation process under vacuum. The resulting green powder was filtered off,
189 washed with 10 mL of cold methanol and dried on air. Suitable green crystals were obtained in two days
190 by slow diffusion of hexane in a DMF solution of 6. Yield: 112 mg (65%).

191 Method B. To a colourless solution of HPip (333 mg, 2.00 mmol) in MeOH:DMF (2.5:1, 50 mL), the
192 green powder Cu(OAc)₂·H₂O (200 mg, 1.00 mmol) was added portion wise and stirred under reflux
193 conditions for 24 h. Colour change from green to dark blue. The resultant solution was treated as
194 mentioned before. Yield: 40.5 mg (75%). Elem. Anal. Calc. for C₄₄H₄₈Cu₂N₄O₂₀ (1079.94 g/mol): C
195 48.93; H 4.48; N 14.01. Found: C 48.72; H 4.35; N 13.97%. ATR-FTIR (wavenumber, cm⁻¹): 2914(br)
196 [ν al(CeH)], 1678(m) [ν (C]O)]DMF, 1661(m) [ν (C]O)]DMF, 1630(m), 1589(m/s) [ν as(COO)], 1497(m),
197 1487(m), 1437(s) [ν s(COO)], 1381(s), 1259(s), 1242(s), 1112(m) [ν (CeOeC)], 1081(m), 1027(s)
198 [δ ip(CeH)], 917(s), 805(m), 773(s) and 679(s) [δ oop(CeH)], 588(m). UV-Vis: (MeOH:DMF (2.5:1),
199 $9.8 \cdot 10^{-4}$ M) λ_{\max} (ϵ)=717 (76) nm.

200

201

202

203

204 2.2.7. [Cu(Pip)2(2-Bzpy)]2 (7)

205 Method A. To a green solution of 1 (100 mg, 0.156 mmol) and HPip (51.9 mg, 0.313 mmol) in MeOH
206 (40 mL), a yellowish solution of 2-Bzpy (0.50 mL, 0.311 mmol) in MeOH (10 mL) was added dropwise
207 and stirred under reflux conditions for 73 h. The dark green solution was treated with sequential cooling-
208 evaporating cycles and a green powder was formed. The powder was filtered. Suitable green crystals
209 were obtained in five days by diffusion of the mother liquors in hexane. Yield: 50.5 mg (48%).

210 Method B. To a green solution of 6 (100 mg, 0.093 mmol) in MeOH (40 mL), a yellowish solution of 2-
211 Bzpy (0.30 mL, 0.186 mmol) in MeOH (10 mL) was added dropwise and stirred under reflux conditions
212 for 24 h. The resulting solution was evaporated under vacuum until dryness and oil was formed. Crude
213 oil was washed several times with hexane and remains vacuumed until a dark green powder was
214 obtained. Yield: 52.3 mg (50%). Elem. Anal. Calc. for C₅₆H₄₀Cu₂N₂O₁₆ (1125.99 g/mol): C 58.53; H
215 4.44; N 4.40. Found: C 58.39; H 4.33; N 4.31%. ATR-FTIR (wavenumber, cm⁻¹): 3082(w) [var(CeH)],
216 2895(w) [val(CeH)], 1634(m), 1594(s) [vas(COO)], 1569(m), 1501(m), 1486(m), 1437(s) [vs(COO)],
217 1386(s), 1256(s), 1240(m), 1170(m), 1110(m) [v(CeOeC)], 1078(m), 1036(s) [δip(CeH)], 924(m),
218 877(w), 804(m), 770(s) [δoop(CeH)], 743(m), 721(m), 700(m), 683(s) [δoop(CeH)], 613(m), 584(m).
219 UV-Vis: (MeOH, 1.1·10⁻³ M) λ_{max} (ε)=689 (86) nm.

220

221 2.3. X-ray single-crystal diffraction analysis

222 The crystallographic data of complexes 2-4a and 5-7 are gathered in tables 1 and 2, respectively.
223 Suitable crystals for X-ray diffraction were obtained by evaporation of mother liquors for 2-5, by
224 DMF:hexane diffusion for 6 and by MeOH:hexane diffusion for 7. The Xray intensity was measured on
225 a D8 Venture system equipped with a multilayer mono-chromate and a Mo microfocus (λ=0.71073 Å).
226 A blue needle-like (2-4a), violet prism-like (5) and green prism-like (6, 7) were used for the X-ray
227 crystallographic analysis. Frames were integrated with the Bruker SAINT Software package using a
228 narrow-frame algorithm. The structures were solved using the Bruker SHELXTL Software, packaged
229 and refined using SHELX (version-2018/3) [23]. Data were corrected for absorption effects using the
230 multi-scan method (SADABS, version 2008/1). Crystal data and additional details of structure
231 refinement for compounds 2-7 are included in the ESI (X-Ray crystal structures). Molecular graphics
232 were generated using Mercury 3.9 software [24,25]. Colour codes for all molecular graphics are: orange
233 (Cu), blue (N), red (O), grey (C) and white (H). Crystal structure and molecular geometry is available in
234 CIF format: CCDC 1851976-1851981 (2-7).

235

236 3. RESULTS AND DISCUSSION

237

238 3.1. General

239 The heteroleptic core compound $[\text{Cu}(\mu\text{-Pip})(\mu\text{-OAc})(\text{MeOH})]_2$ (1) was unexpectedly obtained in our
240 group with 73% yield [18]. As a continuation of this study, in this paper the preparation and
241 characterization of this compound with an 89% of yield is presented. The synthesis consists in the
242 addition of solid $\text{Cu}(\text{OAc})_2 \cdot \text{H}_2\text{O}$ over the HPip in MeOH as solvent. Addition of acetic acid to the
243 reaction media did not affect the reaction product (see experimental). As mentioned in the introduction
244 section, there are few reported examples of Cu(II)-paddlewheel complexes with heteroleptic core and
245 their reactivity has not been described [6–16]. Herein, we present the reactivity study of a heteroleptic
246 core compound with N-donor ligands.

247 Once 1 has been synthesised and fully characterized, its reactivity against pyridine (py, 2), 3-
248 phenylpyridine (3-Phpy, 3), 4-acetylpyridine (4-Acpy, 4a) and 3,5-dimethylpyrazole (3,5-dmpz, 5) in
249 MeOH as solvent at r.t. (2, 3) or reflux (4a, 5) has been performed, resulting in four monomeric
250 compounds: $[\text{Cu}(\text{Pip})_2(\text{dPy})_2(\text{H}_2\text{O})]$ (dPy=py (2), 3-Phpy (3) and 4-Acpy (4)) and $[\text{Cu}(\text{Pip})_2(3,5\text{-}$
251 $\text{dmpz})_2]$ (5) in moderate yields (48–82%). Compound 3 has been previously reported by our research
252 group [17] using a different synthetic approach and in a very low yield (12%). In opposite, here we
253 synthesise it as powder with a 56% of yield. The reactivity of 1, against N-donor ligands, shows that
254 $[\text{Cu}(\mu\text{-Pip})(\mu\text{-OAc})]_2$ core is destroyed, resulting in monomeric compounds. The acetate ligands are
255 displaced from 1, regardless of the pyridine/pyrazole ligands used, and Pip ligands remain coordinated
256 to the metal centre. In complexes 2-4a the five-membered Cu(II) coordination sphere is completed by a
257 water molecule and two pyridine derived ligands. In complex 5, the six-membered coordination sphere
258 is fulfilled by the pyrazole ligand and the bidentate chelate coordination mode of the two Pip ligands on
259 its own (Scheme 1).

260 The reaction of 1 with HPip in MeOH:DMF (2.5:1) as solvent under reflux conditions yields
261 $[\text{Cu}(\text{Pip})_2(\text{DMF})]_2 \cdot 2\text{DMF}$ (6). This compound displays a homoleptic core paddle-wheel structure with
262 DMF molecules in the apical positions. Most interestingly, the reaction between 6 and 2-benzylpyridine
263 (2-Bzpy) in MeOH as solvent under reflux conditions results in $[\text{Cu}(\text{Pip})_2(2\text{-Bzpy})]_2$ (7), which
264 maintains its paddle-wheel structure (Scheme 1). Compound 7 is also obtained from 1 by its reaction
265 with HPip in presence of 2-Bzpy.

266 All compounds were characterized by single crystal X-ray diffraction and analytical and spectroscopic
267 techniques. Spectroscopic characterization details of all compounds are in the experimental section and
268 in the S.I. For complexes, 1–3, 5–7, phase purity of the bulk samples was confirmed by powder X-ray
269 diffraction (PXRD) (S.I.: Fig. S1-S7). Elemental analyses for these compounds agree with the proposed
270 formula. For compound 4, PXRD and elemental analyses are in accordance with the formula
271 $[\text{Cu}(\text{Pip})_2(4\text{-Acpy})_2(\text{H}_2\text{O})]$ (4b) due to the loss of solvent molecules (3 MeOH and H₂O).

272 The IR spectra of compounds 1–7 display the characteristic carboxylate bands in the range 1593–1550
273 cm^{-1} for $\nu(\text{COO})$ and 1442–1356 cm^{-1} for $\nu_s(\text{COO})$. The difference between these bands
274 ($\Delta = \nu(\text{COO}) - \nu_s(\text{COO})$) [26,27] for dimeric compounds 1, 6 and 7 is 151, 154 and 157 cm^{-1} ,
275 respectively, indicating a bridging coordination mode (S.I.: Fig. S8, S13 and S14, respectively). For
276 compounds 2–4 the values of Δ are 200, 207 and 212 cm^{-1} , respectively, corresponding to a
277 monodentate coordination mode (S.I.: Fig. S9 – S11, respectively). Finally, for compound 5 this value is
278 122 cm^{-1} , which indicates a bidentate chelate coordination mode of the carboxylate moieties (S.I.: Fig.
279 S12). The bands attributable to the aromatic groups, $\nu(\text{C}=\text{C})_{\text{ar}}$, $\nu(\text{C}=\text{N})_{\text{ar}}$, $\delta(\text{C}=\text{H})_{\text{ip}}$ and $\delta(\text{C}=\text{H})_{\text{oop}}$,
280 are also present [28]. The presence of solvent molecules allows further identification of some specific
281 bands. Compound 1 shows the $\nu(\text{O}=\text{H})_{\text{MeOH}}$ at 3301 cm^{-1} and 2–4 the $\nu(\text{O}=\text{H})_{\text{water}}$ bands appears in
282 the range 3312–3241 cm^{-1} . Also the $\delta(\text{O}=\text{H})$ can be assigned in these four compounds. Moreover, for
283 compounds 4 and 6, bands attributable to $\nu(\text{C}=\text{O})$ from 4-AcPy (4a, 4b) or DMF (6) units appear in the
284 range 1696–1661 cm^{-1} . The IR spectral data, therefore, agree with the structures determined by the X-
285 ray single-crystal diffraction method.

286

287 3.2. Structural studies

288 3.2.1. Crystal and extended structure of compounds 2-4a Compounds 2-4a crystallize in the monoclinic
289 $C2/c$ space group. They have a monomeric structure with a $[\text{CuO}_3\text{N}_2]$ core comprising a pair of each
290 monodentate ligands, Pip and dpy (py (2) (Fig. 1a), 3-Phpy (3) (Fig. 1b) or 4-AcPy (4a) (Fig. 1c)) and a
291 water molecule. There are >1500 structures [29] with this core and only sixteen of these contain two
292 oxygen atoms from a pair of carboxylates and one from a water molecule [5]. Five-coordinate
293 compounds can adopt trigonal bipyramidal ($D3h$), square-pyramidal ($C4v$) or intermediate ($C2v$)
294 geometries. Several parameters are established to distinguish between them: the value which range from
295 1 ($D3h$) to 0 ($C4v$) [30], the Lapical- M-Lbasal angle (102° for $C4v$) or the dihedral angles between the
296 apical faces (53.1° for $D3h$, 75.7° for $C4v$) and the apical-basal faces (101.5° for $D3h$, 119.8° for $C4v$)
297 [31]. All these compounds clearly exhibit a $C4v$ geometry, taking into account these three factors:
298 (0.205 (2), 0.053 (3), 0.282 (4a)), L-M-L angle (Cu-N1, 97.32° (2), Cu-N1, 93.58° (3), Cu-N1, 95.92°)
299 and dihedral angles (apical faces: 60.22° - 79.35° (2), 62.29° - 76.24° (3), 61.16° - 78.29° (4a); apical-
300 basal: 120.11° - 120.27° (2), 121.14° - 121.02° (3), 120.58° - 121.19° (4a)). The apical sites of the square-
301 pyramidal geometries are occupied by water molecules (Cu-O5, 2.282(9) Å (2), 2.241(3) Å (3), 2.266(6)
302 Å (4a)) while the basal plane contains the supplementary ligands in trans disposition.

303 All the Cu-O and Cu-N distances for the three compounds are in the same order as described in the
304 literature [17,32–36] (Table 3). For 2, Cu(II) ion is 0.109 Å displaced out of the basal plane towards the
305 axial site while in 3 and 4a, Cu(II) ion is displaced 0.029 Å and 0.062 Å, respectively. The twisting of
306 the N-donor ligands produces these displacements and deviation increases $2 > 4a > 3$.

307 Compounds 2-4a, present supramolecular 1D-chains (2, 3) along the b axis (Fig. 2a and 3a, respectively)
308 or 2D-layers (4a) along the bc plane (Fig. 4a).

309 The 1D linear chain formation is supported by two symmetrically bridging interactions in which apical
310 water molecule acts as a heteromeric intermolecular synthon through hydrogen bond interaction with the
311 non-coordinated carboxylate oxygen atoms. These hydrogen bond interactions are moderately strong
312 with D-H \cdots A distances (O5-H5 \cdots O2, 1.90(15) Å (2); 1.87(2) Å (3); 1.97(8) Å (4a)) and bond angles
313 (167(18)° (2), 170(3) (3), 172(14)° (4a)), which are characteristic of strong interactions [37]. Moreover,
314 compound 2 presents a hydrogen bond interaction between two Pip units stacked in a row: one dioxole
315 oxygen atom and the hydrogen of the neighbouring piperonylate aromatic ring (C9-H9 \cdots O4, 2.325(8) Å,
316 166(18)°). This interaction is driven by the carboxylates spatial disposition that supports the
317 supramolecular expansion (Fig. 2b). In contrast, the twisting of the Pip units in 3 and 4a confers a too
318 forced angle (C18-H18 \cdots O3, 2.655 Å, 127.58° (3) and C7-H7 \cdots O3, 2.646 Å, 133.95° (4a)) and avoids
319 the Hbond interaction formation (Fig. 3b). Furthermore, the addition of the acetyl group in 4a allows the
320 formation of supplementary interactions: one aliphatic hydrogen of the acetyl group interacts with the
321 oxygen atom of the dioxole ring propagating the 1D chain along the c axis and forming 2D layers along
322 the bc plane. Interestingly, there are few structures with similar 1D chain with a double H-bond
323 interaction belonging from water – carboxylate [17,32–36], which distinguishes compound 4a from the
324 rest is the presence of three methanol and one occluded water molecules. Its supramolecular 2D square-
325 grid extended structure (Fig. 4b) generates channels that are filled by guest methanol and water solvent
326 molecules. The solvent accessible volume of these channels is a 6.2% of the cell volume. Under air
327 exposure, the guest solvent is lost, as indicated by elemental analysis results, although aqua ligand is
328 not. PXRD of the aerated sample denotes that the initial crystal structure has been modified (S.I.: Fig.
329 S4). Unfortunately, these changes seem to provoke the collapse of the pores, and the material does not
330 adsorb any significant amount of nitrogen.

331

332 3.2.2. Crystal and extended structure of compound 5

333 Compound 5 crystallizes in the triclinic P-1 space group with two crystallographically independent units
334 enclosed in the unit cell (molecules A and B). Each unit has a monomeric structure with a [CuO4N2]
335 core (Fig. 5a) comprising a pair of carboxylate units with a syn-syn chelate array (Cu-O 1.965 Å – 2.653
336 Å) and a pair of monodentate 3,5-dmpz moieties (Cu-N 1.975 Å – 1.977 Å). It has an inversion centre at
337 the metal node, which relates the two carboxylates and the two 3,5-dmpz ligands. This compound
338 presents a distorted octahedral molecular geometry with a significant Oax-Cu-Oeq angle deviation (A,
339 55.02° and 124.98°; B, 55.90° and 124.10°). The equatorial plane is comprised by two shorter distance
340 carboxylate oxygen atoms (O1A and O1B) and two pyrazolic nitrogen atoms (N1A and N1B), which are
341 in range of other reported compounds described in the literature [Cu(Hdmpz)2(L)2] (L=4-
342 methylbenzoate, 3-methylbenzoate, 2-chlorobenzoate, 4-methoxybenzoate [3]; [Cu(C4H4O5)
343 (C5H8N2)2(H2O)]·2H2O [38], [Cu4Cl2(oxalate)(pz)2((1-hydroxymethyl) pyrazole)2]n [39] (Table 4).
344 The asymmetric furthest oxygen atoms [40–44], which are typically generated in chelate carboxylates
345 due to the Jahn-Teller effect [45] occupy the axial sites. In addition, this six coordinate array is

346 underpinned by the elongation of the CeO carboxylic bond length (C1A-O2A 1.247 Å, C1B-O2B 1.248
347 Å) respect to the CeO bond of the uncoordinated piperonylic acid (1.214–1.223 Å), clearly suggesting
348 that this oxygen is coordinated [44].

349 The propagation of intermolecular interactions defines 1D chains along the a axis with all the ligands
350 stacked in a row (Fig. 5b). The main association in this system is the N-pyrazolic donor–carboxylate,
351 which generates a double H-bond interaction. The protonated nitrogen of the pyrazole ring interacts with
352 the coordinated carboxylic oxygen of the asymmetric chelate with the largest Cu–O distance (N2A-
353 H2A··O2A, 1.940(14) Å, 154.10°(15)) forming this kind of supramolecular chains (Table 5).

354

355 3.2.3. Crystal structures of compounds 6 and 7

356 Compounds 6 (Fig. 6a) and 7 (Fig. 6b) crystallize in the triclinic P-1 space group. These compounds are
357 dimers with four symmetrically located ligand moieties orientated in a syn-syn bidentate bridging mode
358 with the carboxylic oxygen atoms coordinating two Cu(II) nodes and anchoring the paddle-wheel-like
359 structure. In both compounds, each Cu (II) node has a square-pyramidal geometry consisting in one
360 apical DMF (6) or 2-Bzpy (7) moiety and four oxygen atoms from the bridging carboxylate groups at
361 the basal plane.

362 Selected distances and angles are provided in Table 6. Compound 6 has the apical units (Cu1-O9) at
363 2.1540(15) Å while compound 7 (Cu1B-N1B) at 2.243(8) Å. The remaining Cu-O distances of the basal
364 plane are in the range 1.959(6) Å and 1.982(7) Å, which are shorter than apical N atoms due to the Jahn-
365 Teller effect [45] but comparable to similar paddle-wheel structures described in the literature (1.945 Å
366 to 2.008 Å) [17,22,46–51].

367 For compound 7, two crystallographically independent dimeric molecules (A and B) are present in the
368 unit cell. In both structures, Cu(II) ions are displaced from the oxygen atoms plane (0.182 Å (6); 0.212
369 Å (7)) towards the apical position. In addition, the square base angles range from 87.45° to 169.37° with
370 a slight deviation of the square-planar geometry ($= 0.0035$ (6) and $= 0.0072$ (7)) [33]. The Cu··Cu
371 intermolecular distances are 2.6057(5) Å and 2.656(1) Å, (6 and 7, respectively). In 6, this Cu··Cu
372 distance is a little bit shorter than other similar structures (2.610 Å–2.713 Å) [17,22,45–50]. It is
373 worthwhile to mention that compound 7 presents the largest angle (O2A–Cu1A–N1A, 99.40°), which
374 corresponds to the carboxylate oxygen closest to the 2-Bzpy ligand. The steric hindrance of
375 the benzyl rings could promote its orientation and the angle opening of the nearest carboxylate ligand
376 (Fig. 6b).

377

378 3.2.4. Extended structures of compounds 6 and 7

379 For compound 6, all the intermolecular interactions are based on coordinated and the uncoordinated
380 DMF molecules. The first intermolecular interaction is the homomeric asymmetric amide–amide
381 interaction between them (C5-H5B··O9, 2.407(3) Å; C5-H5B, 0.9900(14) Å; C5··O9, 3.314(4) Å,
382 152.11° (6)). The following interactions are between aliphatic proton from each of two Pip units and an

383 uncoordinated DMF molecule through its carboxylic oxygen atom, which also interacts with a
384 coordinated DMF of a neighbouring paddle-wheel forming 1D chains along the a axis (C19-
385 H19B··O10, 2.102(4) Å; C19-H19, 0.9800(14) Å; C19··O19, 3.036(4) Å, 158.54° (6)) (Fig. 7a). The
386 remaining pair of Pip units interacts directly with a coordinated DMF molecule of another neighbouring
387 paddle-wheel (Fig. 7b) generating 2D layers along the (00½) plane (C13-H13A··O10, 2.163(4) Å; C13-
388 H13A, 0.9900(16) Å; C13··O10, 3.096(3) Å, 156.57° (7)). For compound 7, the 2D supramolecular
389 structure is generated by the propagation in the bc plane through two alternated simultaneous hydrogen
390 bond interactions. Each dimeric unit possesses four propagation centres, two from the 2-Bzpy units (Fig.
391 8a) and two from the piperonylate units (Fig. 8b). These two crystallographically different 2-Bzpy rings
392 interacts with the oxygen atoms of the neighbouring dioxole Pip rings (C16-H16··O8, 2.511(3) Å; C16-
393 H16 0.9500(14) Å; C16··O8, 3.213(3) Å and C4- H4··O15, 2.513(3) Å; C4-H4 0.9500(14) Å; C4··O15,
394 3.165(3) Å) and constructing 2D layer.

395

396 3.3. UV–Vis spectroscopy

397 UV–Vis electronic spectra for all the compounds have been recorded in methanol (1–5, 7) or
398 MeOH:DMF (2.5:1) (6) as solvent. All spectra show one band in the visible region, between 727 and
399 677 nm with $\epsilon = 13\text{--}124\text{M}^{-1}\text{cm}^{-1}$ (S.I.: Fig. S15). For a d9 ion, with a 2D term, there is only one
400 transition between the two levels 2Eg and 2T2g. In the octahedral crystalline field, the spin-orbital
401 coupling unfolds the 2T2g level in two sublevels due to its tetragonal distortion (Jahn-Teller effect). For
402 these reasons, an octahedral d9 ion has two possible transitions, both from the 2Eg level to each of the
403 unfolded 2T2g sublevels giving two absorption bands. However, in the case of Cu(II) these sublevels are
404 energetically close and the difference in energy is too small to discriminate between them resulting in a
405 broad band [52,53]. The energy of these electronic transitions depends on the fulfilment of the two
406 selection rules (Laporte and spin). Electronic transitions in d9 Cu(II) complexes only accomplish the
407 spin rule, for this reason the energy of this transitions is lower than other transition metal complexes and
408 its ϵ values range from 10 to 200M⁻¹ cm⁻¹. The obtained values for compound 1–7 are in accordance
409 with the values reported in the literature for similar Cu(II) complexes (Table 7) [18,54–57].

410

411

412 **4. CONCLUSIONS**

413

414 The reactivity of the heteroleptic core compound 1 with selected supplementary ligands (py, 3-Phpy, 4-
415 Acpy and 3,5-dmpz) results in the rupture of the dimeric array and yields monomeric species (2–5). In
416 opposite, the reaction between the homoleptic core compound 6 with the 2-Bzpy ligand yield the
417 dimeric compound 7, keeping the paddlewheel building unit. It is worthwhile to mention that even
418 though there are similar heteroleptic core previously described in the literature [6–16], there are few
419 studies about their reactivity. In this juncture, besides presenting the first trial in this sense, it is also
420 remarkable the different behaviour exhibited by the two paddle-wheel compounds (1, 6). This difference
421 can only be promoted by the fact of having mixed bridges.

422

423 **ACKNOWLEDGEMENTS**

424

425 This work was financed by the Spanish National Plan of Research MAT2015-65756-R, CTQ2016-
426 75150-R and 2017SGR1687, 2014SGR149 projects from the Generalitat de Catalunya for its financial
427 support.

428

429 **REFERENCES**

430

- 431 [1] J.M. Lehn, *Chem. Soc. Rev.* 36 (2007) 151–160.
- 432 [2] L. Zhao, F. Guo, *J. Coord. Chem.* 66 (2013) 2940–2947.
- 433 [3] S.W. Jin, X.H. Ye, L. Jin, L. Zheng, J.W. Li, B.P. Jin, D.Q. Wang, *Polyhedron* 81 (2014) 382–
434 395.
- 435 [4] B. Olenyuk, M.D. Levin, J.A. Whiteford, J.E. Shield, P.J. Stang, *J. Am. Chem. Soc.* 121 (1999)
436 10434–10435.
- 437 [5] C.R. Groom, I.J. Bruno, M.P. Lightfoot, S.C. Ward, *Acta Crystallogr. Sect. B Struct. Sci. Cryst.*
438 *Eng. Mater.* 72 (2016) 171–179.
- 439 [6] K. Hassanein, O. Castillo, C.J. Gómez-García, F. Zamora, P. Amo-Ochoa, *Cryst. Growth Des.*
440 15 (2015) 5485–5494.
- 441 [7] I. Galkina, A. Tufatullin, D. Krivolapov, Y. Bakhtiyarova, D. Chubukaeva, V. Stakheev, V.
442 Galkin, R. Cherkasov, B. Büchner, O. Kataeva, *CrystEngComm* 16 (2014) 9010–9024.
- 443 [8] B. Kozlevčar, D. Odlazek, A. Golobič, A. Pevec, P. Strauch, P. Šegedin, *Polyhedron* 25 (2006)
444 1161–1166.
- 445 [9] W. Ying, L. Xiao-Meng, B. Feng-Ying, Z. Rui, *Chinese, J. Inorg. Chem.* 33 (2017) 1667–1677.
- 446 [10] G. Vives, S.A. Mason, P.D. Prince, P.C. Junk, J.W. Steed, *Cryst. Growth Des.* 3 (2003) 699–
447 704.
- 448 [11] D. MasPOCH, D. Ruiz-Molina, K. Wurst, C. Rovira, J. Veciana, *Chem. Commun.* (2002) 2958–
449 2959.
- 450 [12] D. MasPOCH, D. Ruiz-Molina, K. Wurst, J. Vidal-Gancedo, C. Rovira, J. Veciana, *Dalton Trans.*
451 7 (2004) 1073–1082.
- 452 [13] L.S. Erre, G. Micera, P. Piu, F. Cariati, G. Ciani, *Inorg. Chem.* 24 (1985) 2297–2300.
- 453 [14] A.A. Ageshina, M.A. Uvarova, S.E. Nefedov, *Russ. J. Inorg. Chem.* 60 (2015) 1085–1092.
- 454 [15] M.A. Bañares, L. Dauphin, X. Lei, W. Cen, M. Shang, E.E. Wolf, T.P. Fehlner, *Chem. Mater.* 7
455 (1995) 553–561.

- 456 [16] J.-H. Luo, C.-C. Huang, X.-H. Huang, J.-G. Wang, *Acta Crystallogr. Sect. C Cryst. Struct.*
457 *Commun.* 64 (2008) m121–m122.
- 458 [17] J. Soldevila-Sanmartín, J.A. Ayllón, T. Calvet, M. Font-Bardia, J. Pons, *Polyhedron* 126 (2017)
459 184–194.
- 460 [18] J. Soldevila-Sanmartín, J.A. Ayllón, T. Calvet, M. Font-Bardia, C. Domingo, J. Pons, *Inorg.*
461 *Chem. Commun.* 71 (2016) 90–93.
- 462 [19] J. Soldevila-Sanmartín, T. Calvet, M. Font-Bardia, C. Domingo, J.A. Ayllón, J. Pons, *Dalton*
463 *Trans.* 47 (2018) 6479–6493.
- 464 [20] M. Sanchez-Sala, J. Pons, Á. Álvarez-Larena, C. Domingo, J.A. Ayllón, *ChemistrySelect* 2
465 (2017) 11574–11580.
- 466 [21] M. Guerrero, S. Vázquez, J.A. Ayllón, T. Calvet, M. Font-Bardia, J. Pons, *ChemistrySelect* 2
467 (2017) 632–639.
- 468 [22] M. Barquín, N. Cocera, M.J. González Garmendia, L. Larrínaga, E. Pinilla, M.R. Torres, J.
469 *Coord. Chem.* 63 (2010) 2247–2260.
- 470 [23] G.M. Sheldrick, *Acta Crystallogr. Sect. A Found. Crystallogr.* 64 (2007) 112–122.
- 471 [24] C.F. Macrae, P.R. Edgington, P. McCabe, E. Pidcock, G.P. Shields, R. Taylor, M. Towler, J.
472 Van De Streek, *J. Appl. Crystallogr.* 39 (2006) 453–457.
- 473 [25] C.F. Macrae, I.J. Bruno, J.A. Chisholm, P.R. Edgington, P. McCabe, E. Pidcock, L. Rodriguez-
474 Monge, R. Taylor, J. Van De Streek, P.A. Wood, *J. Appl. Crystallogr.* 41 (2008) 466–470.
- 475 [26] K. Nakamoto, *Infrared and Raman, Spectra of Inorganic and Coordination Compounds Part A :*
476 *Theory and Applications*, 6th ed., John Wiley & Sons, New York, USA, 2009.
- 477 [27] R.J. Deacon, G.B. Phillips, *Coord. Chem. Rev.* 33 (1980) 227–250.
- 478 [28] D.H. Williams, *Spectroscopic methods in organic chemistry*, McGraw-Hill, London, UK, 2008.
- 479 [29] Cambridge Structural, Database (CSD), (Version 5.37) (2016).
- 480 [30] A.W. Addison, T.N. Rao, *J. Chem. Soc., Dalton. Trans.* 1 (1984) 1349–1356.
- 481 [31] E..L. Muetterties, *Tetrahedron* 30 (1973) 1595–1604.

- 482 [32] Y. Li, X. Meng, L. Cao, Y. Wang, G. Yin, M. Gao, L. Wen, A. Wu, *Cryst. Growth Des.* 8
483 (2008) 1645–1653.
- 484 [33] F. Valach, R. Grobelny, T. Glowiak, J. Mrozinski, V. Lukeš, Z. Blahova, *J. Coord. Chem.* 63
485 (2010) 1645–1651.
- 486 [34] S. Jin, H. Liu, G. Chen, Z. An, Y. Lou, K. Huang, D. Wang, *Polyhedron* 95 (2015) 91–107.
- 487 [35] J. Moncol', M. Palicová, P. Segl'a, M. Koman, M. Melník, M. Valko, T. Glowiak, *Polyhedron*
488 21 (2002) 365–370.
- 489 [36] F. Hamza, G. Kickelbick, *Macromolecules* 42 (2009) 7762–7771.
- 490 [37] T. Steiner, *Angew. Chem., Int. Ed.* 41 (2002) 49–76.
- 491 [38] Y.-L. Wang, G.-J. Chang, B.-X. Liu, *Acta Cryst., E* 67 (2011) m682 m682.
- 492 [39] A.M. López Marzo, M. Guerrero, T. Calvet, M. Font-Bardia, E. Pellicer, M.D. Baró, J. Pons, J.
493 Sort, *RSC Adv.* 5 (2015) 32369–32375.
- 494 [40] J. Moncol, K. Jomova, L. Zelenicky, T. Lis, M. Valko, *Acta Cryst., C* 67 (2011) 318–320.
- 495 [41] U. Turpeinen, R. Hämäläinen, J. Reedijk, *Inorg. Chim. Acta* 154 (1988) 201–207.
- 496 [42] J. Valdés-Martínez, R.A. Toscano, J. Ramirez-Ortíz, *Polyhedron* 14 (1995) 579–583.
- 497 [43] A.F. Cameron, K.P. Forrest, D.W. Taylor, R.H. Nuttall, *J. Chem. Soc. (A)* (1971) 2492–
498 2496.
- 499 [44] S. Ščavničar, B. Matković, *Acta Crystallogr Sect. B Struct. Crystallogr. Cryst. Chem.* 25 (1969)
500 2046–2055.
- 501 [45] L.R. Falvello, *J. Chem. Soc., Dalt. Trans.* 1 (1997) 4463–4475.
- 502 [46] M. Guerrero, J.A. Ayllón, T. Calvet, M. Font-Bardia, J. Pons, *Polyhedron* 134 (2017) 107–113.
- 503 [47] P.M. Selvakumar, S. Nadella, J. Sahoo, E. Suresh, P.S. Subramanian, *J. Coord. Chem.* 66 (2013)
504 287–299.
- 505 [48] N. Lah, G. Giester, P. Šegedin, A. Murn, K. Podlipnik, I. Leban, *Acta Cryst., C* 57 (2001) 546–
506 548.

- 507 [49] M. Barquín, M.J. González-Garmendia, L. Larrínaga, E. Pinilla, J.M. Seco, M.R. Torres, J.
508 Coord. Chem. 63 (2010) 1652–1665.
- 509 [50] S. Youngme, A. Cheansirisomboon, C. Danvirutai, C. Pakawatchai, N. Chaichit, C. Engkagul,
510 G.A. van Albada, J.S. Costa, J. Reedijk, Polyhedron 27 (2008) 1875–1882.
- 511 [51] T. Kawata, H. Uekusa, T. Furukawa, T. Tokii, Y. Muto, M. Kato, S. Ohba, Acta Crystallogr.
512 Sect. B 48 (1992) 253–261.
- 513 [52] J.E. Huheey, E.A. Keiter, R.L. Keiter, Inorganic chemistry. Principles of Structure and
514 Reactivity, 4th Ed., Harper Collins College Publishers, New York, USA, 1993.
- 515 [53] D. Sutton, Electronic Spectra of Transition Metal Complexes, McGraw-Hill, London, UK, 1975.
- 516 [54] S. Kumar, R.P. Sharma, P. Venugopalan, V. Singh Gondil, S. Chhibber, T. Aree, M. Witwicki,
517 V. Ferretti, Inorg. Chim. Acta 1 (2018) 288–297.
- 518 [55] R.P. Sharma, A. Saini, S. Kumar, J. Kumar, P. Venugopalan, V.S. Gondil, S. Chhibber, T. Aree,
519 Polyhedron 123 (2017) 430–440.
- 520 [56] N. Wei, N.N. Murthy, K.D. Karlin, Inorg. Chem. 33 (1994) 6093–6100.
- 521 [57] L.-L. Han, S.-N. Wang, Z. Jagličić, S.-Y. Zeng, J. Zheng, Z.-H. Li, J.-S. Chen, D. Sun,
522 CrystEngComm 17 (2015) 1405–1415.

524 **Legends to figures**

525

526 **Scheme 1** Schematic synthesis of the compounds 1–7.

527

528 **Figure. 1** Molecular structure of $[\text{Cu}(\text{Pip})_2(\text{dPy})_2(\text{H}_2\text{O})]$ (a $\text{dPy}=\text{py}$ (2); b 3-Phpy (3); c 4-Acpy (4))
529 complexes showing an atom labelling scheme. The hydrogen atoms are omitted for clarity.

530

531 **Figure. 2 a.** a axis view of the one-dimensional ordering of the $[\text{Cu}(\text{Pip})_2(\text{py})_2(\text{H}_2\text{O})]$ (2) complex by
532 water-carboxylate hydrogen bonding through the b axis. **b.** Piperonylate ligands stacked in a row
533 disposition allows its intermolecular $\text{C}_\text{e}\text{H}\cdots\text{O}$ hydrogen bonding interactions.

534

535 **Figure. 3 a.** a axis view of the one-dimensional ordering of the $[\text{Cu}(\text{Pip})_2(3\text{-Phpy})_2(\text{H}_2\text{O})]$ (3) complex
536 by water-carboxylate hydrogen bonding through the b axis. **b.** Piperonylates planarity drifting
537 disposition prevent its intermolecular $\text{C}_\text{e}\text{H}\cdots\text{O}$ hydrogen bonding. Only hydrogens involved in the
538 intermolecular interaction are shown.

539

540 **Figure. 4 a.** a axis view of the one-dimensional ordering of the $[\text{Cu}(\text{Pip})_2(4\text{-}$
541 $\text{Acpy})_2(\text{H}_2\text{O})]\cdot 3\text{MeOH}\cdot\text{H}_2\text{O}$ (4a) complex by water-carboxylate hydrogen bonding through the b axis.
542 **b.** b axis view of the propagation through the bc plane by hydrogen bonding between the oxygen of the
543 piperonylate units and the protons of the acetyl groups. Solvent molecules are omitted for clarity.

544

545 **Figure. 5 a.** Molecular structure of $[\text{Cu}(\text{Pip})_2(3,5\text{-dmpz})_2]$ (5) complex showing an atom labelling
546 scheme. The hydrogen atoms are omitted for clarity. **b.** b axis view of the one-dimensional ordering of
547 the $[\text{Cu}(\text{Pip})_2(3,5\text{-dmpz})_2]$ (5) complex by a double pirazole-carboxylate hydrogen bonding forming 1D
548 chains. Only hydrogen atoms involved in the intermolecular interactions are shown.

549

550 **Figure. 6 a.** Molecular structure of $[\text{Cu}(\text{Pip})_2(\text{DMF})_2]$ (6). **b.** Molecular structure of $[\text{Cu}(\text{Pip})_2(2\text{-}$
551 $\text{Bzpy})_2]$ (7) complexes showing an atom labelling scheme. The hydrogen atoms are omitted for clarity

552

553 **Figure. 7 a.** b axis view of the one-dimensional ordering through the coordinated DMF molecules and
554 the Pip rings of the $[\text{Cu}(\text{Pip})_2(\text{DMF})_2]$ (6). **b.** ab view of the onedimensional ordering through the
555 uncoordinated DMF molecules joining two dimeric units of $[\text{Cu}(\text{Pip})_2(\text{DMF})_2]\cdot 2\text{DMF}$. Only hydrogen
556 atoms from DMF molecules and those involved in the intermolecular interaction are shown.

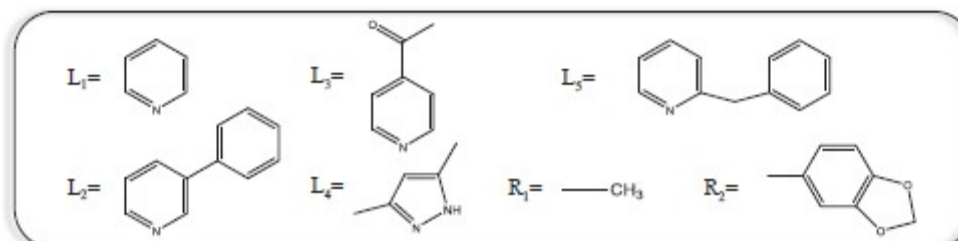
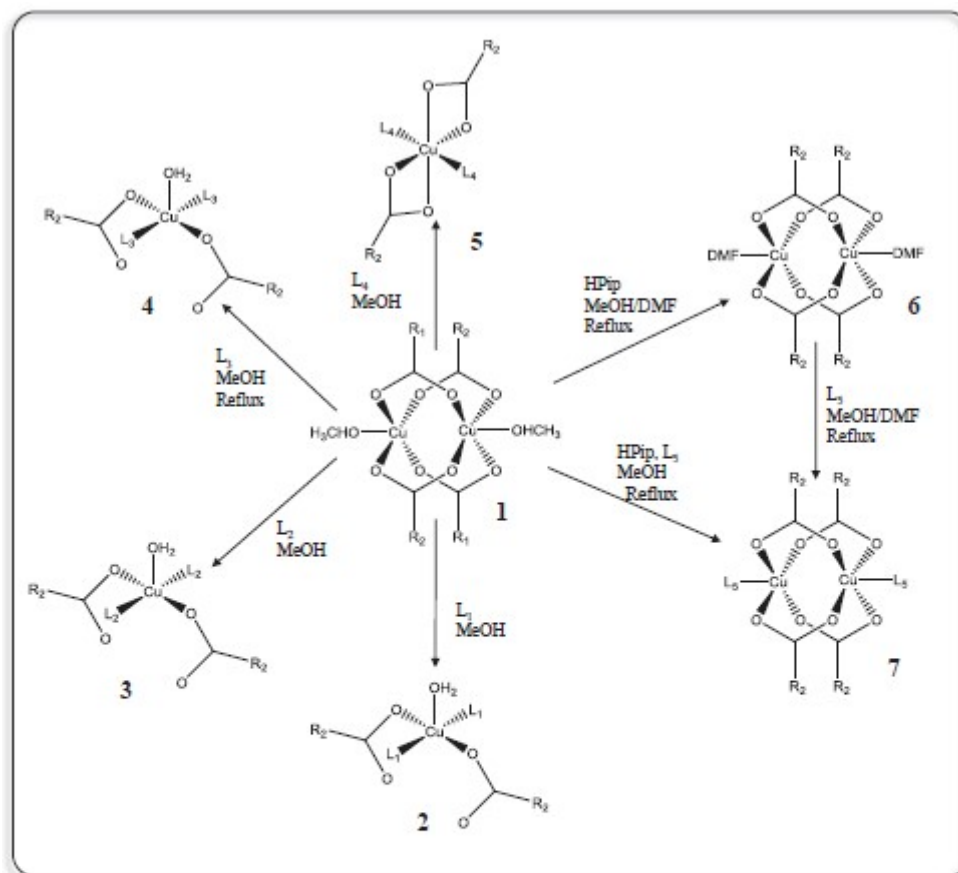
557

558 **Figure. 8 a** and b shows the $\text{C}_\text{e}\text{H}\cdots\text{O}$ hydrogen bonding formation of compound 7 between the Pip rings
559 and the pyridil ring of the 2-Bzpy units forming the 2D layers. **a.** $(1/3\ 1/2\ 1)$ view and **b.** $(1/3\ 1\ 1/2)$
560 view of these weak interactions.

561 SCHEME 1

562

563

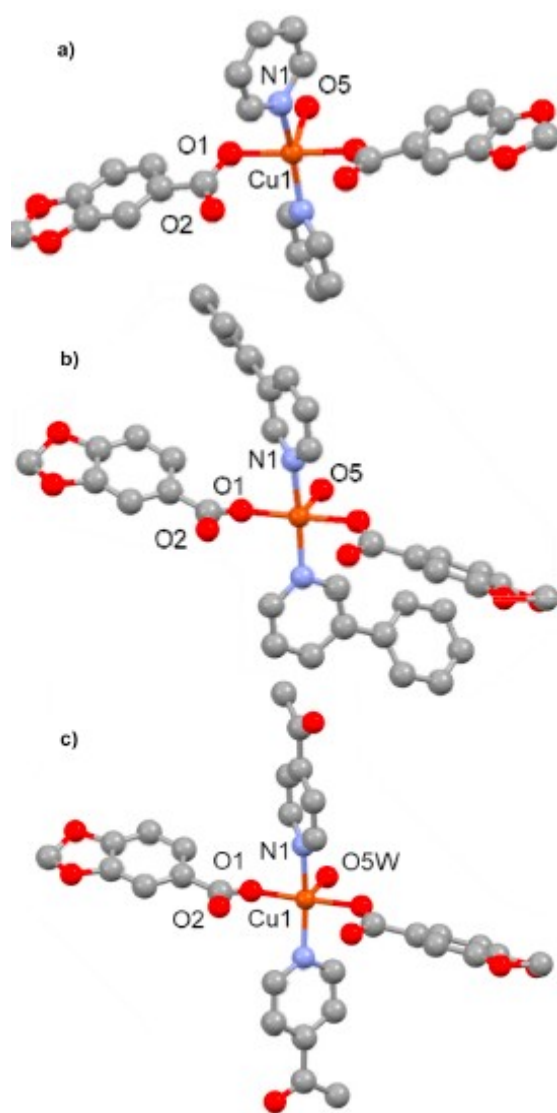


564

565

566
567
568

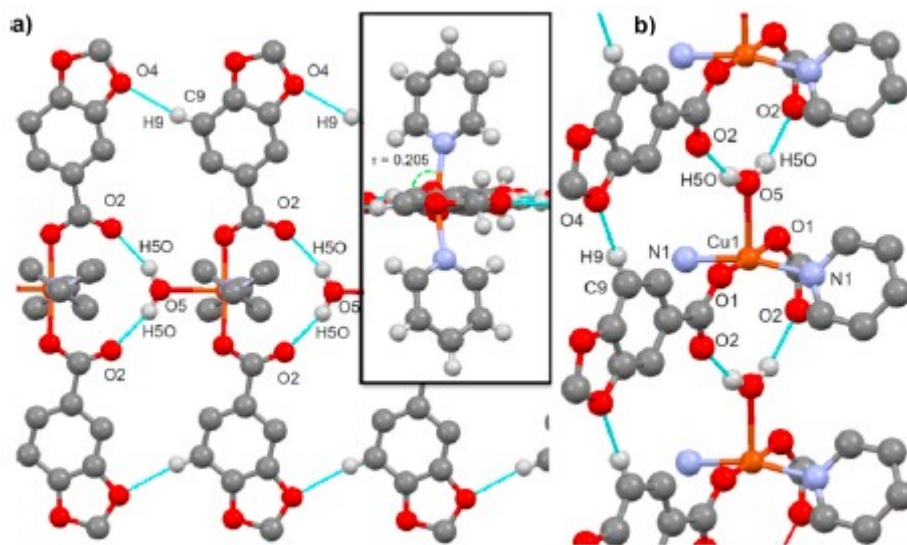
FIGURE 1



569
570

571
572
573

FIGURE 2



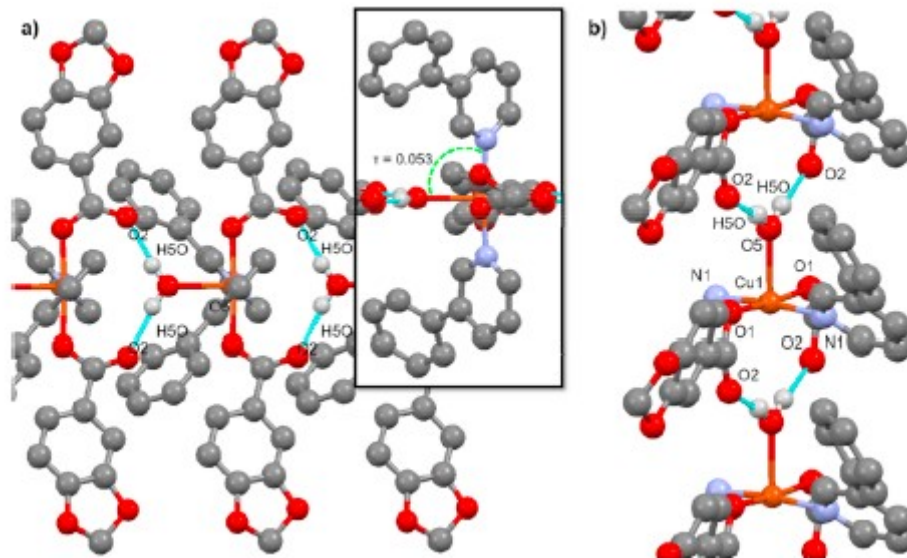
574
575

576

FIGURE 3

577

578



579

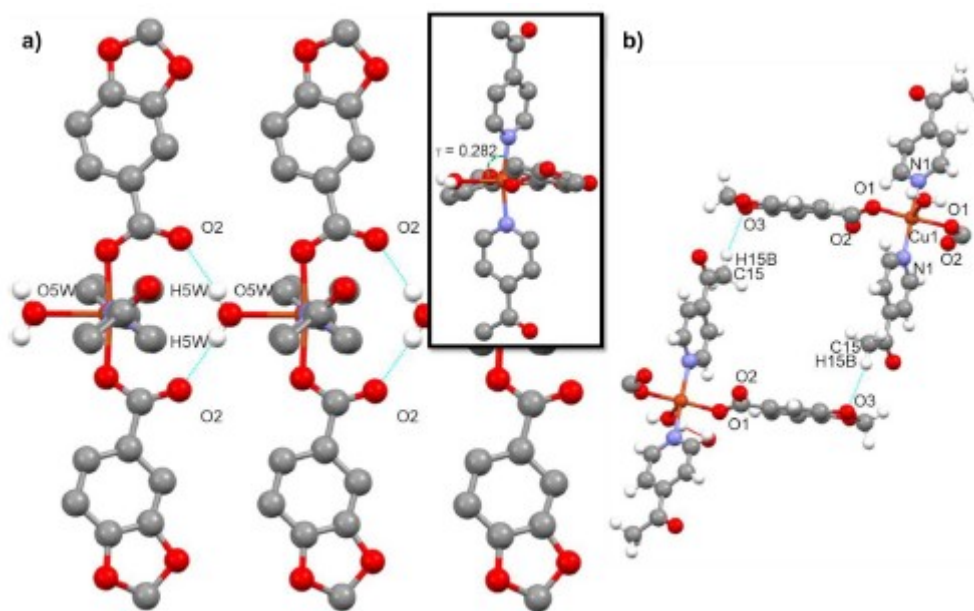
580

581

FIGURE 4

582

583

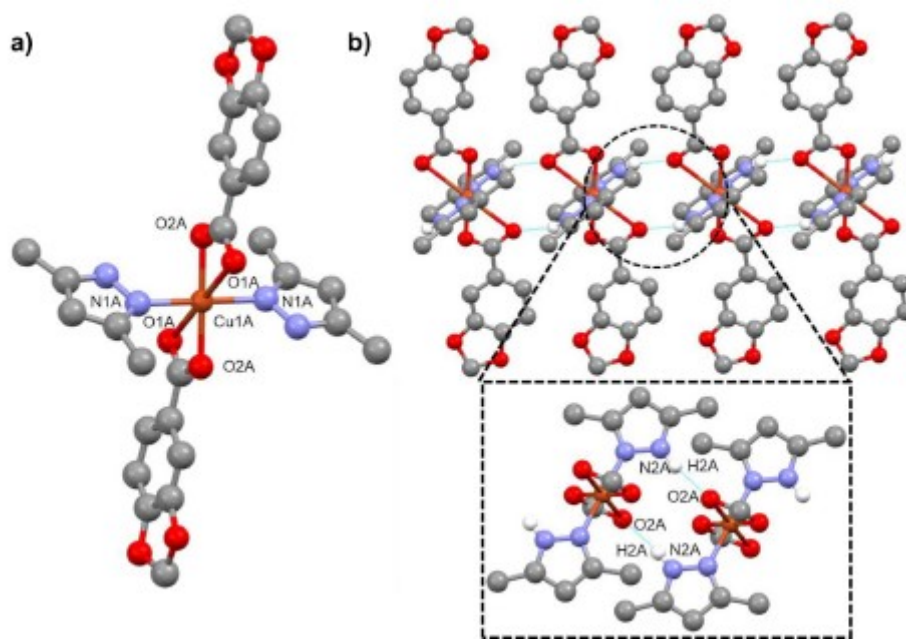


584

585

586
587
588

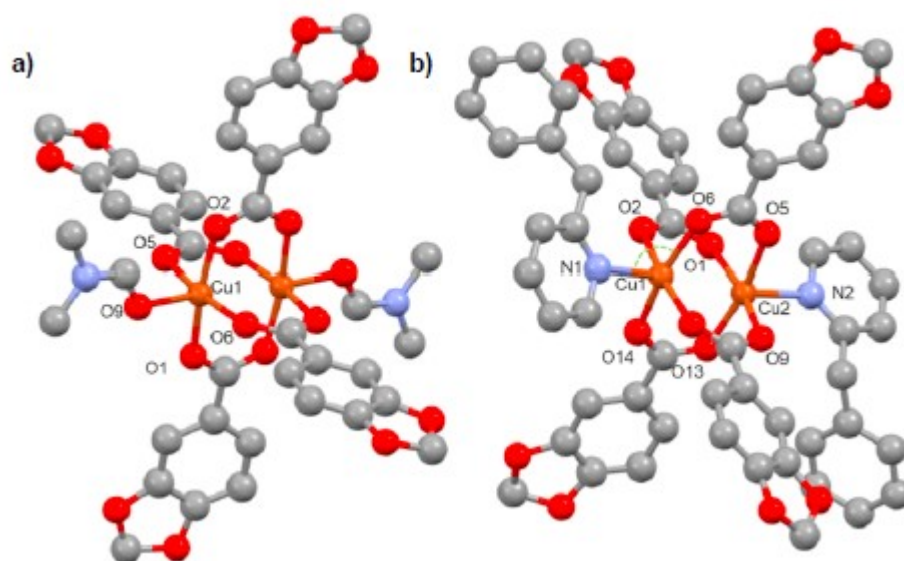
FIGURE 5



589
590

591
592
593

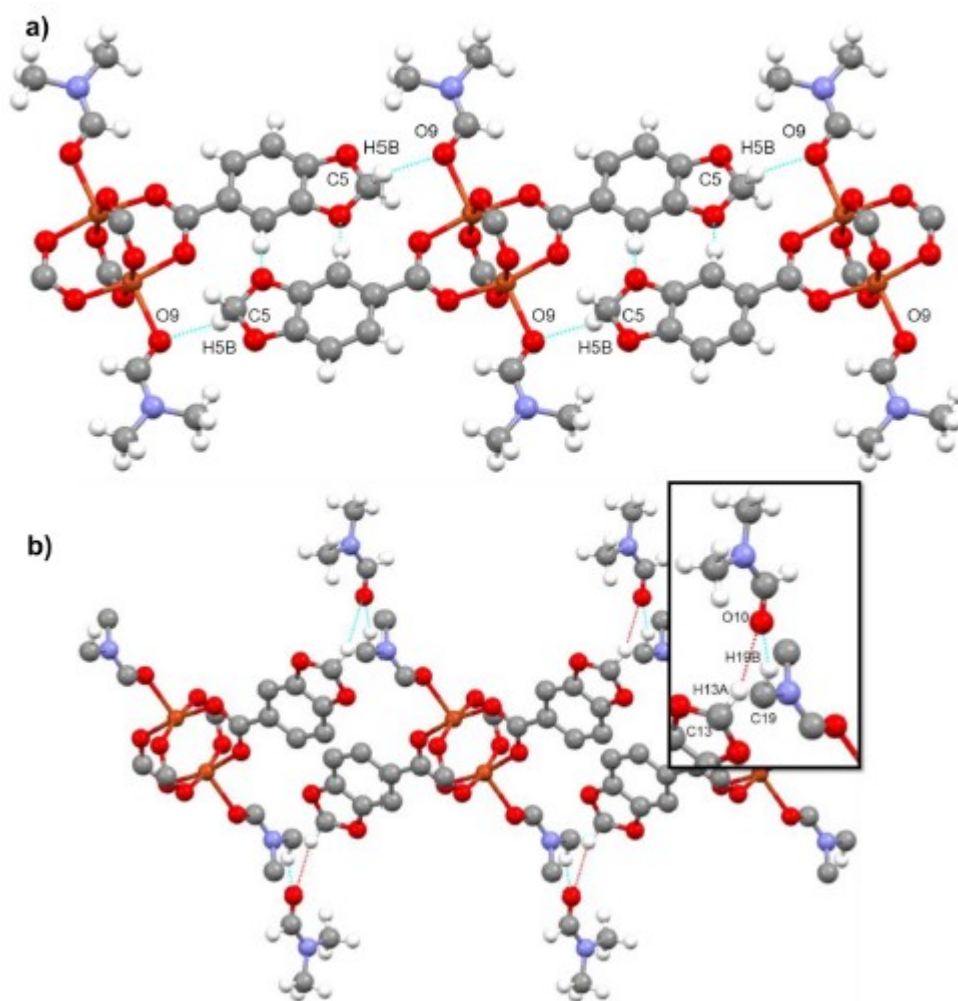
FIGURE 6



594
595

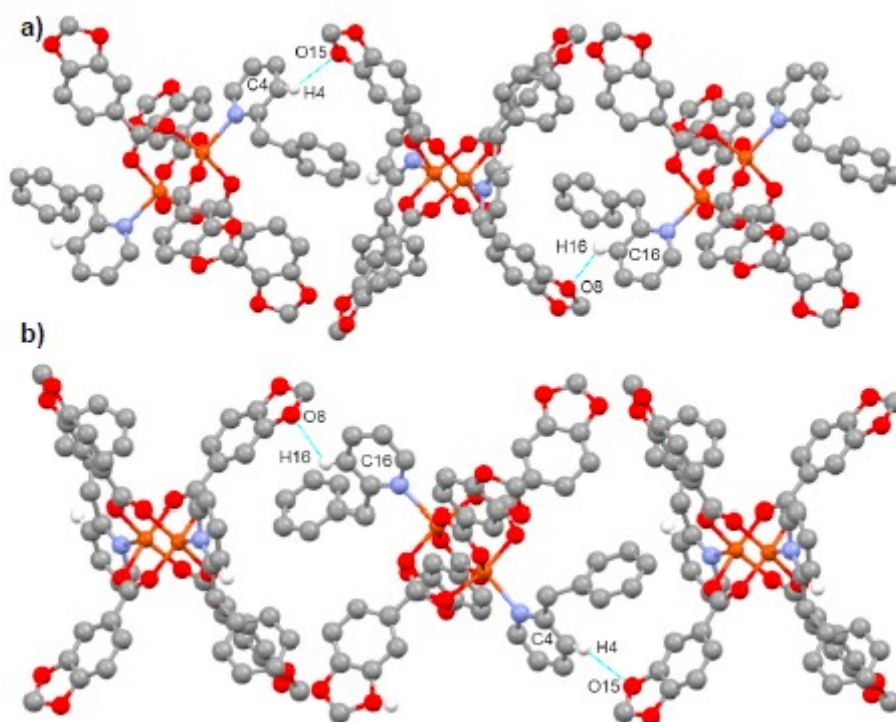
596
597
598

FIGURE 7



599
600

FIGURE 8



601
602
603

604
605

606 **Table 1** Crystallographic data for compounds 2–4.

607

	2	3	4
Empirical formula	C ₃₂ H ₂₂ CuN ₂ O ₆	C ₃₈ H ₃₀ CuN ₂ O ₆	C ₃₉ H ₄₀ CuN ₂ O ₁₅
Formula weight	569.99	722.20	768.21
T (K)	100(2)	100(2)	100(2)
Wavelength (Å)	0.71073	0.71073	0.71073
System, space group	Monoclinic, C 2/c	Monoclinic, C 2/c	Monoclinic, C 2/c
Unit cell dimensions			
a (Å)	15.530(3)	22.6648(13)	23.1610(17)
b (Å)	6.1225(12)	5.7527(3)	5.8928(4)
c (Å)	25.132(5)	23.9870(16)	26.0634(19)
α (°)	90	90	90
β (°)	91.533(6)	95.958(4)	110.439(2)
γ (°)	90	90	90
V (Å ³)	2388.7(8)	3110.6(3)	3333.3(4)
Z	4	4	4
Dcalc (g cm ⁻³)	1.585	1.542	1.531
μ (mm ⁻¹)	0.975	0.767	0.733
F(0 0 0)	1172	1492	1604
Crystal size (mm ³)	0.297x0.063x0.062	0.707x0.101x0.038	0.179x0.068x0.032
hkl ranges	-17 ≤ h ≤ 18 -7 ≤ k ≤ 7 -29 ≤ l ≤ 29	-29 ≤ h ≤ 29 -7 ≤ k ≤ 7 -31 ≤ l ≤ 31	-23 ≤ h ≤ 23 -6 ≤ k ≤ 6 -26 ≤ l ≤ 26
2θ range (°)	3.048 to 24.446		
Reflections collected/unique/[R(int)]	8490/1953 [R(int) = 0.0449]	32090/3576 [R(int) = 0.1365]	51462/1898 [R(int) = 0.0691]
Completeness to θ = 25.242°	99.1%	99.9%	63.0%
Absorption Correction	Semi-empirical	Semi-empirical	Semi-empirical
Max. and min. transmits.	0.7451 and 0.6333	0.7456 and 0.6731	0.7446 and 0.6930
Refinement method	Full matrix least-squares on F ²	Full matrix least-squares on F ²	Full matrix least-squares on F ²
Data/restraints/parameters	1953/1/159	3576/0/230	1898/5/222
Goodness of fit (GOF) on F ²	1.134	1.056	1.084
Final R indices [I > 2σ(I)]	R1 = 0.0853, wR2 = 0.2283	R1 = 0.0518, wR2 = 0.0960	R1 = 0.0675, wR2 = 0.1757
R indices (all data)	R1 = 0.0916, wR2 = 0.2320	R1 = 0.0849, wR2 = 0.1073	R1 = 0.0735, wR2 = 0.1813
Extinction coefficient	n/a	n/a	n/a
Largest. Diff. peak and hole (e Å ⁻³)	2.324 and -1.830	0.423 and -0.661	1.623 and -0.761

608

609

610

611 **Table 2** Crystallographic data for compounds 5–7.

612

	5	6	7
Empirical formula	C ₂₆ H ₂₀ CuN ₄ O ₈	C ₄₄ H ₄₀ Cu ₂ N ₄ O ₂₀	C ₅₆ H ₄₂ Cu ₂ N ₂ O ₁₆
Formula weight	586.05	1079.94	1125.99
T (K)	100(2)	100(2)	100(2)
Wavelength (Å)	0.71073	0.71073	0.71073
System, space group	Triclinic, P-1	Triclinic, P-1	Monoclinic, P21/c
Unit cell dimensions			
a (Å)	6.0789(2)	10.4359(5)	17.0709(6)
b (Å)	12.4827(4)	11.1697(5)	18.5452(7)
c (Å)	17.7198(6)	12.1119(6)	15.3980(5)
α (°)	73.0490(10)	87.276(2)	90
β (°)	83.9550(10)	65.220(2)	99.8320(10)
γ (°)	86.468(2)	64.078(2)	90
V (Å ³)	1278.35(7)	1136.84(10)	4803.2(3)
Z	2	1	4
Dcalc (g cm ⁻³)	1.523	1.577	1.557
μ (mm ⁻¹)	0.913	1.023	0.965
F(0 0 0)	606	558	2312
Crystal size (mm ³)	0.236x0.138x0.081	0.233x0.158x0.155	0.278x0.082x0.045
hkl ranges	-7 ≤ h ≤ 7 -15 ≤ k ≤ 15 -22 ≤ l ≤ 22	-14 ≤ h ≤ 13 -15 ≤ k ≤ 15 -17 ≤ l ≤ 17	-22 ≤ h ≤ 22 -24 ≤ k ≤ 24 -20 ≤ l ≤ 20
2θ range (°)	2.413 to 26.728	2.421 to 30.557	2.422 to 28.332
Reflections collected/unique/[R(int)]	29716/5397 [R(int) = 0.0345]	46461/6939 [R(int) = 0.0305]	122091/11916 [R(int) = 0.0495]
Completeness to θ = 25.242°	99.6%	99.7%	99.4%
Absorption Correction	Semi-empirical	Semi-empirical	Semi-empirical
0.7454 and 0.6940	0.7454 and 0.6940	0.7461 and 0.6897	0.7457 and 0.6985
Refinement method	Full matrix least-squares on F ²	Full matrix least-squares on F ²	Full matrix least-squares on F ²
Data/restraints/parameters	5397/0/359	6939/0/317	11916/1/685
Goodness of fit (GOF) on F ²	1.020	1.036	1.048
Final R indices [I > 2σ(I)]	R1 = 0.0293, wR2 = 0.0714	R1 = 0.0427, wR2 = 0.1060	R1 = 0.0359, wR2 = 0.0893
R indices (all data)	R1 = 0.0384, wR2 = 0.0761	R1 = 0.0516, wR2 = 0.1119	R1 = 0.0488, wR2 = 0.0976
Extinction coefficient	n/a	n/a	n/a
Largest. Diff. peak and hole (e Å ⁻³)	0.464 and -0.419	1.480 and -1.465	0.623 and -0.567

613

614

615 **Table 3** Selected bond lengths (Å) and bond angles (°) for compounds 2 – 4a.

616

2			
Bond length (Å)			
Cu(1)-O(1)	1.937(5)	Cu(1)-N(1)	2.018(6)
Cu(1)-O(1)#1	1.937(5)	Cu(1)-N(1)#1	2.017(6)
Cu(1)-O(5)	2.282(9)		
Bond angles (°)			
O(1)#1-Cu(1)-O(1)	177.7(3)	O(1)#1-Cu(1)-N(1)#1	90.5(2)
O(1)#1-Cu(1)-O(5)	88.86(16)	N(1)#1-Cu(1)-O(5)	97.3(2)
O(1)#1-Cu(1)-N(1)	89.8(2)	N(1)-Cu(1)-N(1)#1	165.5(4)
O(1)#1-Cu(1)-O(5)	88.86(16)		
3			
Bond length (Å)			
Cu(1)-O(1)	1.9379(19)	Cu(1)-N(1)	2.020(2)
Cu(1)-O(1)#1	1.9380(19)	Cu(1)-N(1)#1	2.020(2)
Cu(1)-O(5)	2.241(3)		
Bond angles (°)			
O(1)-Cu(1)-O(1)#1	176.06(14)	O(1)-Cu(1)-O(5)	88.03(7)
O(1)-Cu(1)-N(1)	91.72(9)	N(1)-Cu(1)-O(5)	93.62(8)
O(1)#1-Cu(1)-N(1)	88.53(9)	N(1)#1-Cu(1)-O(5)	93.62(8)
N(1)-Cu(1)-N(1)#1	172.77(15)		
4a			
Bond length (Å)			
Cu(1)-O(1)	1.928(4)	Cu(1)-N(1)	2.023(5)
Cu(1)-O(1)#1	1.928(4)	Cu(1)-N(1)#1	2.023(5)
Cu(1)-O(5W)	2.266(6)		
Bond angles (°)			
O(1)-Cu(1)-O(1)#1	174.9(3)	O(1)-Cu(1)-O(5W)	87.47(13)
O(1)#1-Cu(1)-N(1)#1	91.64(18)	N(1)#1-Cu(1)-O(5W)	95.92(15)
O(1)#1-Cu(1)-N(1)	88.88(18)	N(1)-Cu(1)-N(1)#1	168.2(3)

617

2: #1 -x + 1,y,-z + 3/2; 3: #1 -x + 1,y,-z + 1/2; 4: #1 -x + 1,y,-z + 1/2;

618

619 **Table 4** Selected bond lengths (Å) and bond angles (°) for compound 5.

620

5			
Bond length (Å)			
Cu(1A)-O(1A)#1	1.9654(12)	Cu(1B)-O(1B)#2	1.9672(12)
Cu(1A)-O(2A)	2.6536(14)	Cu(1B)-O(2B)	2.6138(14)
Cu(1A)-N(1A)#1	1.9749(15)	Cu(1B)-N(1B)#2	1.9769(15)
Bond angles (°)			
O(1A)#1-Cu(1A)-O(1A)	180	O(1B)#2-Cu(1B)-O(1B)	180
O(1A)#1-Cu(1A)-N(1A)	89.78(6)	O(1B)#2-Cu(1B)-N(1B)	89.74(6)
O(1A)#1-Cu(1A)-N(1A)	90.22(6)	O(1B)#2-Cu(1B)-N(1B)	90.26(6)
#1		#2	
N(1A)-Cu(1A)-N(1A)#1	180	N(1B)-Cu(1B)-N(1B)#2	180

5: #1 -x,-y,-x + 1 #2 -x + 2,-y + 1,-x + 2.

621

622

623

624 **Table 5** Selected intermolecular interactions for compounds 2–5.

625

2	H–A (Å)	D–A (Å)	D–H (Å)	> D–H–A (°)
O5–H5O–O2	1.90(15)	2.802(8)	0.92(12)	167(18)
O9–H9–O4	2.325(8)	3.253(15)	0.9500	166(18)
3				
O5–H5O–O2	1.87(2)	2.711(3)	0.85(3)	170(3)
4a				
O5W–H5W–O2	1.967(8)	2.765(13)	0.804(10)	171.62(14)
C15–H15B–O3	2.470(12)	3.433(14)	0.9800(12)	167.74(14)
5				
N2A–H2A–O2A	1.940(14)	2.7588(12)	0.8800(14)	154.10(15)
N2B–H2B–O2B	1.977(14)	2.7615(12)	0.8800(14)	147.76(15)

626

627

628 **Table 6** Selected bond lengths (Å) and bond angles (°) for compounds 6 and 7.

629

6			
Bond length (Å)			
Cu(1)-O(5)#1	1.9633(14)	Cu(1)-O(2)#1	1.9727(13)
Cu(1)-O(1)	1.9669(13)	Cu(1)-O(9)	2.1540(15)
Cu(1)-O(6)	1.9695(14)	Cu-Cu	2.6057(5)
Bond angles (°)			
O(5)#1-Cu(1)-O(1)	88.98(6)	O(6)-Cu(1)-O(9)	92.64(6)
O(5)#1-Cu(1)-O(6)	169.37(6)	O(2)#1-Cu(1)-O(9)	95.08(6)
O(1)-Cu(1)-O(6)	91.69(6)	O(5)#1-Cu(1)-Cu(1)#1	89.85(5)
O(5)#1-Cu(1)-O(2)#1	88.44(6)	O(1)-Cu(1)-Cu(1)#1	83.70(4)
O(1)-Cu(1)-O(2)#1	169.17(6)	O(6)-Cu(1)-Cu(1)#1	79.68(4)
O(6)-Cu(1)-O(2)#1	88.94(6)	O(2)#1-Cu(1)-Cu(1)#1	85.78(4)
O(5)#1-Cu(1)-O(9)	97.86(6)	O(9)-Cu(1)-Cu(1)#1	172.26(5)
O(1)-Cu(1)-O(9)	95.69(6)		
7			
Bond length (Å)			
Cu(1)-O(6)	1.9516(14)	Cu(2)-O(13)	1.9598(14)
Cu(1)-O(14)	1.9588(14)	Cu(2)-O(5)	1.9722(14)
Cu(1)-O(2)	1.9731(14)	Cu(2)-O(9)	1.9773(14)
Cu(1)-O(10)	1.9785(14)	Cu(2)-O(1)	1.9835(14)
Cu(1)-N(1)	2.1999(16)	Cu(2)-N(2)	2.2484(16)
		Cu(1)-Cu(2)	2.6910(3)
Bond angle (°)			
O(6)-Cu(1)-O(14)	166.18(6)	O(13)-Cu(2)-O(5)	167.61(6)
O(6)-Cu(1)-O(2)	89.11(7)	O(13)-Cu(2)-O(9)	87.99(6)
O(14)-Cu(1)-O(2)	88.84(7)	O(5)-Cu(2)-O(9)	91.71(6)
O(6)-Cu(1)-O(10)	90.28(6)	O(13)-Cu(2)-O(1)	88.68(7)
O(14)-Cu(1)-O(10)	88.87(7)	O(5)-Cu(2)-O(1)	88.51(6)
O(2)-Cu(1)-O(10)	167.89(6)	O(9)-Cu(2)-O(1)	165.36(6)
O(6)-Cu(1)-N(1)	95.73(6)	O(13)-Cu(2)-N(2)	99.01(6)
O(14)-Cu(1)-N(1)	98.08(6)	O(5)-Cu(2)-N(2)	93.11(6)
O(2)-Cu(1)-N(1)	101.49(6)	O(9)-Cu(2)-N(2)	103.37(6)
O(10)-Cu(1)-N(1)	90.60(6)	O(1)-Cu(2)-N(2)	91.23(6)

6: #1-x + 2,-y,-z + 1.

630

631

632 **Table 7** UV–Vis spectroscopy data of compounds 1–7 and similar examples of the literature.
633

Compound	Geometry	λ_{max} (nm)	ϵ (M^{-1} cm^{-1})	Ref.
[Cu(dien)(pnb) ₂] \cdot H ₂ O	sqp	615	194	[54]
[Cu(dien) ₂](pnb) ₂	Oh	618	120	[54]
[Cu(dien)(pnb)(H ₂ O)] \cdot (pnb) \cdot (Hpnb)	sqp	608	140	[54]
[Cu(en) ₂ (H ₂ O) ₂](2-PBA) ₂ \cdot 2H ₂ O	Oh	546	–	[55]
[Cu(en) ₂ (H ₂ O)] \cdot (DPA) ₂ \cdot 3H ₂ O	sqp	535	–	[55]
[TMpA)CuCl] ⁺	bpt	725	90	[56]
[(BPQA)CuCl] ⁺	sqp	700	106	[56]
[(BQPA)CuCl] ⁺	sqp	737	137	[56]
[(TMQA)CuCl] ⁺	sqp	691	185	[56]
[Cu(μ -Pip)(μ -Ac)(MeOH)] ₂ (1)	sqp	716	124	[18]
[Cu(Pip) ₂ (py) ₂ (H ₂ O)] (2)	sqp	710	33	work
[Cu(Pip) ₂ (3-Phpy) ₂ (H ₂ O)] (3)	sqp	727	78	work
[Cu(Pip) ₂ (4-Acpy) ₂ (H ₂ O)] (4)	sqp	677	68	work
[Cu(Pip) ₂ (3,5-dmpx) ₂] (5)	Oh	714	13	work
[Cu(μ -Pip) ₂ (DMF)] \cdot 2DMF (6)	sqp	717	76	work
[Cu(μ -Pip) ₂ (2-Bzpy)] (7)	sqp	689	86	work

dien = diethylenetriamine; Hpnb = *p*-nitrobenzoic acid; en = ethylenediamine; PBA = phenoxybenzoate; DPA = diphenylacetate; TMpA = tris[[(2-pyridyl)methyl]]-methylamine; BPQA = 1-(pyridin-2-yl)-*N*-(pyridin-2-yl-methyl)-*N*-(quinolin-2-ylmethyl)methanamine; BQPA = 1-(pyridin-2-yl)-*N,N*-bis(quinolin-2-ylmethyl)methanamine; TMQA = 1-(isoquinolin-3-yl)-*N,N*-bis(quinolin-2-ylmethyl)methanamine. bpt = trigonal-bipyramidal; sqp = square-pyramidal; Oh = octahedral.